Transmission of Solar Radiation by Clouds over Snow and Ice Surfaces: A Parameterization in Terms of Optical Depth, Solar Zenith Angle, and Surface Albedo

MELANIE F. FITZPATRICK

Department of Earth and Space Sciences, University of Washington, Seattle, Washington

RICHARD E. BRANDT

Department of Atmospheric Sciences, University of Washington, Seattle, Washington

STEPHEN G. WARREN

Department of Earth and Space Sciences, and Department of Atmospheric Sciences, University of Washington, Seattle, Washington

(Manuscript received 21 January 2003, in final form 25 June 2003)

ABSTRACT

A multilevel spectral radiative transfer model is used to develop simple but accurate parameterizations for cloud transmittance as a function of cloud optical depth, solar zenith angle, and surface albedo, for use over snow, ice, and water surfaces. The same functional form is used for broadband and spectral transmittances, but with different coefficients for each spectral interval. When the parameterization is applied to measurements of ''raw'' cloud transmittance (the ratio of downward irradiance under cloud to downward irradiance measured under clear sky at the same zenith angle), an ''effective'' optical depth τ is inferred for the cloud field, which may be inhomogeneous and even patchy. This effective optical depth is only a convenient intermediate quantity, not an end in itself. It can then be used to compute what the transmittance of this same cloud field would be under different conditions of solar illumination and surface albedo, to obtain diurnal and seasonal cycles of cloud radiative forcing. The parameterization faithfully mimics the radiative transfer model, with rms errors of 1%–2%. Lack of knowledge of cloud droplet sizes causes little error in the inference of cloud radiative properties. The parameterization is applied to pyranometer measurements from a ship in the Antarctic sea ice zone; the largest source of error in inference of inherent cloud properties is uncertainty in surface albedo.

1. Introduction

Clouds have large effects on the earth's radiation budget, both longwave and shortwave. Lack of knowledge of cloud distributions and cloud properties, and of the behavior of clouds during climatic change, limits the accuracy of climate-prediction models (Cess et al. 1990). Cloud distributions and radiative properties are now being monitored from space by the International Satellite Cloud Climatology Project (ISCCP; Rossow and Schiffer 1999). There is also a need for surface measurements of cloud properties to obtain the effects of clouds on the radiation budget at the surface as well as at the top of the atmosphere, and to infer cloud properties in regions where satellite cloud detection is difficult, particularly over snow and ice surfaces.

Field experiments [e.g., the Atmospheric Radiation Measurement (ARM) Program; Stokes and Schwartz 1994] can obtain cloud properties with fine spectral detail at a few geographic locations. However, climate research would benefit if the routine solar radiation measurements made at weather stations worldwide, and on many research ships, using broadband pyranometers, could be used to determine the cloud radiative forcing (CRF) at the surface. Here we investigate what information about clouds can be obtained from broadband measurements, with particular attention to the effect of surface albedo on the measured downward shortwave irradiance.

The number of weather stations measuring solar radiation is a small fraction of the number making visual cloud observations, and the number of research ships is much smaller than the total number of merchant ships making routine weather observations (including cloud observations) at sea. In order that the isolated surface measurements of CRF can be extended to larger areas using a cloud climatology (e.g., Warren et al. 1986, 1988), inherent cloud radiative properties are needed. A value for cloud transmittance can be obtained just by comparing the measured downward solar irradiance be-

Corresponding author address: Melanie F. Fitzpatrick, Department of Earth and Space Sciences, University of Washington, Box 351310, Seattle, WA 98195.
E-mail: fitz@atmos.washington.edu

neath the cloud to that obtained at the same solar zenith angle, θ, on a clear day in the same month. However, this same cloud would have a different measured transmittance if illuminated at a different zenith angle or if positioned over a surface with different albedo, α. To use a cloud climatology to compute surface CRF therefore requires an intermediate quantity that is inherent to the cloud field (which may be inhomogeneous and nonovercast), which can be used to compute transmittance given θ and α. This intermediate quantity is the effective optical depth τ. It is ''effective'' in two senses: (a) it is computed assuming a horizontally homogeneous overcast cloud, and (b) the cloud is assumed to consist of liquid water droplets with a standard effective radius ($r_{\text{eff}} = 8.6$ μm, as explained later). The effective cloud optical depth is the same as the true optical depth if the observed cloud actually is horizontally homogeneous and has $r_{\text{eff}} = 8.6$ μm. In all other cases the effective optical depth is just a convenient intermediate quantity whose utility is determined by its ability to predict the transmittance of the observed cloud field over surfaces and under illumination different from those observed. Such an effective cloud optical depth has been used previously by Barker et al. (1998) and is used by ISCCP (Hahn et al. 2001; Rossow and Schiffer 1999). Boers et al. (2000) showed that errors in true average optical depth retrieved from ground-based pyranometers can be as large as 50% due to cloud inhomogeneities. For this reason we are careful to note our use of optical depth only as an intermediate quantity. It is designed to give the correct transmittance but cannot be expected to give the correct cloud water content.

Several previous studies have determined cloud optical properties in polar atmospheres from ground-based measurements of solar irradiance. In polar regions with snow-covered ground, Shine (1984) and Gardiner (1987) noted that multiple reflection between the snow and the underside of the cloud can increase the radiation received at the surface by a factor of 2. In characterizing clouds, this multiple reflection must be considered. However, Wiscombe (1975) showed that because of the strong spectral variation of cloud albedo and surface albedo, the difference between cloud-top reflectance and cloud-bottom reflectance (spectrally averaged) depends on cloud optical depth, so that simple spectrally averaged multiple-bounce models like Gardiner's cannot accurately relate transmittance of radiation through a cloud to cloud optical depth.

Previous work on inferring cloud optical depth using only broadband measurements was carried out by Leontyeva and Stamnes (1994). They used broadband measurements of downwelling irradiance and surface albedo together with a multilayer radiative transfer model to iteratively determine cloud optical depth. A further study by Leontyeva and Stamnes (1996) determined cloud optical depth from spectral transmittance using lookup tables that had been derived from the radiative transfer model. In both cases good characterization of surface albedo was found to be necessary. Lubin and Simpson (1997) determined cloud scattering optical depth at visible wavelengths using a radiative transfer model to determine the clear sky irradiance. They then iterated with a discrete ordinates model, adjusting the estimated cloud optical depth until the calculated irradiance matched the measured irradiance. All these methods rely on an iterative solution to the radiative transfer equation for each irradiance measurement, a time-consuming process if large quantities of data are to be processed.

To simplify this step, a simple parameterization is presented here that relates cloud transmittance to cloud optical depth, surface albedo, and solar zenith angle. This parameterization can mimic the results of a multilayer, multiwavelength radiative transfer model. We apply this parameterization to obtain cloud properties from radiation measurements made during a ship voyage in the Southern Ocean.

2. Parameterization

We define a quantity, ''raw'' cloud transmittance (trc), that can be obtained from the measurements alone without any model. It is simply the ratio of downward irradiance measured under cloud to that measured under clear sky at the same solar zenith angle. It is this quantity, trc, for which we will derive a parameterization. Using a two stream multiple-reflection model, Wiscombe (1975) motivated the form of a parameterization for Arctic summer stratus clouds, relating cloud transmittance to cloud droplet number density for a grey underlying surface. We have rederived this parameterization using a spectrally varying surface albedo and different cloud drop-size distributions. In the original paper on the two stream method, Schuster (1905) showed that the monochromatic transmittance through a nonabsorbing, isotropically scattering atmosphere of optical depth τ is just $1/(1 + \tau)$. Wiscombe (1975, his Eq. 24) generalized this functional form as $1/(c + dn_c)$, where c and d are empirical coefficients and n_c is cloud droplet number density. We replace cloud droplet number density with cloud optical depth τ, in the geometrics–optics limit, as discussed later. Cloud transmittance is greater if the sun is higher, and Wiscombe (1975) found that a linear function of $\cos\theta$ was adequate to describe this effect. Wiscombe accounted for multiple reflections between cloud and ground by including a spectrally averaged albedo in the denominator as a multiplier of cloud droplet number density. However, Shine (1984) showed that neglecting the spectral variation of high surface albedos leads to an underestimate of surface irradiance. In the radiative transfer model used to develop the parameterization we therefore use a spectrally varying surface albedo, with spectral shapes characteristic of snow and ice surfaces. The broadband parameterization itself uses the spectrally averaged albedo, so it is valid only for surfaces of snow, sea ice, and

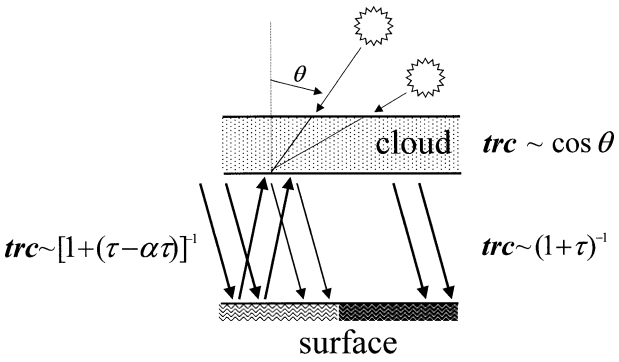

FIG. 1. Schematic diagram of the physical basis of the parameterization. The cloud is underlain by two different surface types: a dark surface on the right and a bright surface, which supports multiple reflections, on the left. The measured raw cloud transmittance, trc, is (i) proportional to the cosine of the solar zenith angle θ, (ii) inversely proportional to cloud optical depth τ, and (iii) increased by multiple reflection between the cloud base and the surface with albedo α.

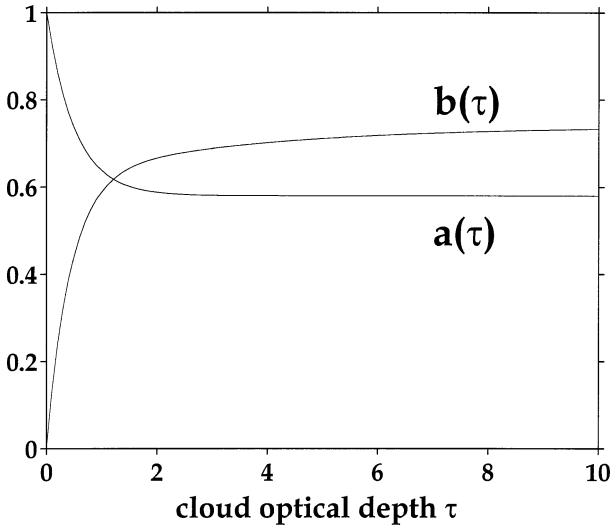

FIG. 2. The functional forms of $a(\tau)$ and $b(\tau)$ used in the broadband parameterization (for $r_{\text{eff}} = 8.6$ μm) to ensure correct asymptotic behavior for both thin clouds and thick clouds.

water; however, the narrowband parameterizations derived next should be generally valid.

Our parameterization is

$$\text{trc} = \frac{a(\tau) + b(\tau)\cos\theta}{1 + (c - d\alpha)\tau}. \quad (1)$$

Figure 1 shows the physical reasoning behind this parameterization. The coefficients a and b were constants in Wiscombe's (1975) parameterization; however, to make the parameterization accurate in the limit of $\tau \to 0$ we found it necessary to make these coefficients functions of τ:

$$a(\tau) = a_1 + (1 - a_1)\exp(-k_1\tau) \quad \text{and} \quad (2)$$

$$b(\tau) = b_1[1 + b_2\exp(-k_2\tau) + b_3\exp(-k_3\tau)]. \quad (3)$$

Figure 2 shows the coefficients $a(\tau)$ and $b(\tau)$: they asymptote to constant values for large τ. At small τ, a approaches 1 and b approaches 0, removing the solar zenith angle dependence of cloud transmittance. We tried a variety of τ dependencies of a and b, including $\ln\tau$ and τ^2, but the best relationship found is an exponential dependence. The coefficients were determined using a nonlinear least squares algorithm (Press et al. 1992, 678–683) separately for each of three different drop-size distributions, covering a range of solar zenith angles, surface albedos, and cloud optical depths.

The optical depth used in (1), and which we attempt to retrieve from measurements of trc, is the geometric–optics optical depth, τ_g; that is, with extinction efficiency $Q_{\text{ext}} = 2$. We use τ_g to describe the clouds because it is a quantity that is independent of wavelength. All forms of the parameterization given later, whether broadband or spectral, have coefficients chosen to give τ_g. The relationship between cloud optical depth and drop-size distribution is given by

$$\tau_g = 2\pi h \int r^2 n(r)\, dr, \quad (4)$$

where h is cloud thickness, r is cloud droplet radius, and $n(r)$ is the cloud drop-size distribution. Effective radius is defined as the ratio of the third moment to the second moment of the particle radius distribution function, and is given by

$$r_{\text{eff}} = \frac{\int r^3 n(r)\, dr}{\int r^2 n(r)\, dr}. \quad (5)$$

A representative drop-size spectrum for Arctic stratus clouds was given by Jayaweera and Ohtake (1973). It has $r_{\text{eff}} = 8.6$ μm. Observed effective radii for springtime cloud droplets in the Southern Ocean range from 4.5 to 16.6 μm (Boers and Krummel 1998). They were measured between 40° and 55°S during the First Aerosol Characterization Experiment (ACE-1), in November and December 1995. No trend was observed in r_{eff} within this latitude range, so these values may also be representative for other parts of the Southern Ocean (R. Boers 2000, personal communication). However r_{eff} is probably smaller in summer than in winter because there are more cloud condensation nuclei in summer (Ayers and Gras 1991).

3. Model

To derive the coefficients of the parameterization we use a multilayer atmospheric radiative transfer model, ATRAD (Wiscombe et al. 1984), with 118 spectral intervals in the UV, visible, and near-infrared. The model assumes a plane-parallel, horizontally homogeneous atmosphere, and neglects polarization. The adding–doubling method is used to compute radiative transfer. Ab-

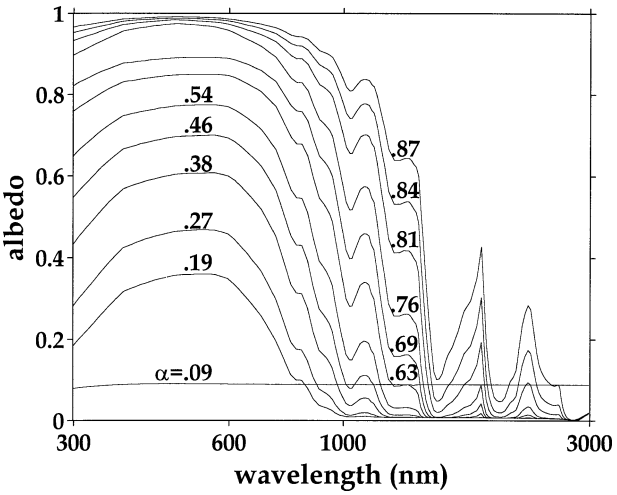

FIG. 3. Spectral albedos used to develop the parameterization for 12 different surfaces, ranging from open water to fine-grained snow for a solar zenith angle of 60° under a clear sky. The labels indicate the spectrally averaged albedo for each surface type under these conditions.

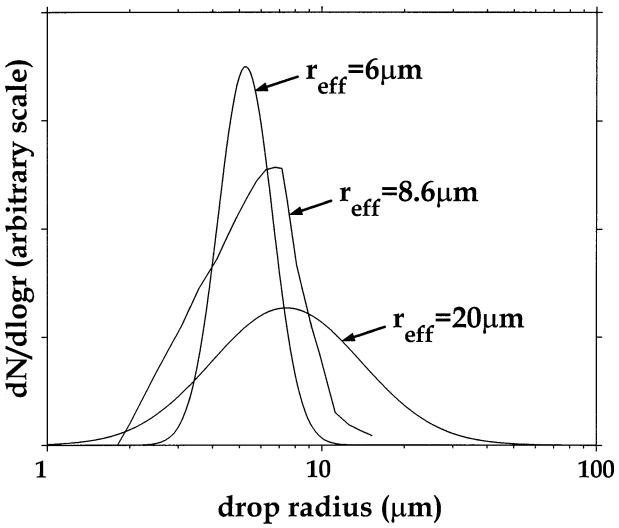

FIG. 4. Three different drop-size distributions used in developing the parameterization. The distribution with $r_{\text{eff}} = 8.6$ μm is an observed distribution measured in Arctic stratus clouds (Jayaweera and Ohtake 1973). The other two are lognormal distributions (Reist 1993, chapter 2).

sorption and scattering by aerosols, clouds, and all natural atmospheric gases are included. Exponential sum fitting of transmittance (ESFT) is used to compute gaseous absorption. Mie theory is used to compute scattering and absorption by cloud droplets, with exact calculations (Wiscombe 1980) performed for size parameters below 100, and approximate calculations (Nussenzveig and Wiscombe 1980) for larger-size parameters.

We used the top-of-atmosphere solar spectrum as given by Labs and Neckel (1970) and Neckel and Labs (1984). For atmospheric profiles of temperature, ozone, and water vapor we used the subarctic summer standard atmosphere (McClatchey et al. 1972) modified to force a relative humidity of 100% (with respect to liquid water) within the cloud. For all optical depths used, the cloud base was placed at 0.6 km and the cloud top at 1.3 km; the optical depth was varied by varying the droplet number density, keeping the cloud thickness fixed. This assumption, as well as the assumption that r_{eff} is independent of height within the cloud, has little effect on the computed trc.

The underlying surface is described by a spectral albedo, 1 of 12 choices shown in Fig. 3; the reflected radiation is distributed with angle according to an azimuthally averaged bidirectional reflectance function given by Warren (1982, his Fig. 15). The 12 spectral albedos are meant to represent surfaces ranging from fine-grained new snow (uppermost curve), through coarse-grained old melting snow, to granular sea ice of decreasing scattering coefficient. The nearly horizontal curve at the bottom is that of open water from Briegleb and Ramanathan (1982), but it more closely resembles the spectral albedo measured for thin nilas by Brandt et al. (1999). These spectral albedos for hypothetical (modeled) surfaces types were used because they are available in the ATRAD model. However, they do resemble spectral albedos measured for snow and for various types of sea ice (Grenfell et al. 1994; Grenfell and Perovich 1984; Brandt et al. 1999).

The spectral and broadband cloud transmittance was computed for three zenith angles ($\cos\theta = 0.2, 0.4, 0.6$), 14 cloud optical depths (τ from 0.02 to 88 with geometric spacing, and $\tau = 0$ for clear sky), and the 12 surface albedos with broadband albedos from 0.09 (open water) to 0.87 (fine-grained snow); a total of 504 different conditions. They were then repeated for the three different drop-size distributions shown in Fig. 4. The standard drop-size distribution is that measured for water droplets in an Arctic stratus cloud by Jayaweera and Ohtake (1973); it has an effective radius of 8.6 μm. The other two drop-size distributions are lognormal distributions with effective radii of 6 and 20 μm.

The parameterization proved difficult to fit to ATRAD results for surface albedos $\alpha \geq 0.83$. Furthermore, the inference of τ becomes increasingly indeterminate as $\alpha \rightarrow 1$. We therefore fitted the coefficients for the parameterization only to model results for $\alpha \leq 0.83$. This is not a severe restriction, as sea ice scenes usually contain some open water or thin ice that lowers the area-averaged albedo.

4. Results

a. Broadband parameterization

A broadband parameterization, covering the solar spectrum from 0.3 to 3.0 μm, so as to cover the spectral range measured by pyranometers, is derived for each of

TABLE 1. Values of coefficients in Eqs. (1), (2), and (3) for the broadband parameterization (0.3–3.0 μm) determined using three different drop-size distributions. The last column gives the root-mean-square difference between values of cloud transmittance obtained from the spectral radiative transfer model and those obtained using the parameterization.

r_{eff}	a_1	b_1	b_2	b_3	k_1	k_2	k_3	c	d	Rms (%)
6.0 μm	0.58	0.75	−0.2053	−0.7935	2.0506	0.1968	2.4790	0.1409	0.1329	1.2
8.6 μm	0.58	0.74	−0.1612	−0.8343	1.9785	0.2828	2.3042	0.1365	0.1291	1.3
20 μm	0.58	0.71	−0.7420	−0.2661	0.5600	0.2881	3.1293	0.1206	0.1133	2.4

the three different drop-size distributions. The values of the coefficients in Eqs. (1), (2), and (3) are listed in Table 1. Cloud transmittance values derived using the parameterization with an effective radius of 8.6 μm show an rms error of 1.3% when compared with values obtained from the radiative transfer model (Fig. 5). A synthetic dataset is used to determine the difference in optical depths obtained from the three different drop-size distributions, using values of trc, $\cos\theta$, and α to derive τ. Figure 6 shows the inferred optical depths that result from different assumptions for the effective radius, at a solar zenith angle of 60° and a surface albedo of 0.55. The comparison was performed for other values of solar zenith angle and surface albedo and a similar percentage variation in τ is obtained. For a given cloud optical depth, a cloud with large particles has greater forward scattering and hence greater cloud transmittance. For the range of observed effective radii in the Southern Ocean, incorrect assumptions of effective radius in the parameterization introduce a 10%–15% error in the inferred effective optical depth.

However, for climatological applications, effective optical depth is simply an intermediate quantity that allows us to find the transmittance of the same cloud field over different surfaces and at different solar zenith angles. The errors introduced in predicted cloud transmittance, caused by assuming an incorrect drop-size distribution, are shown for one example in Fig. 7. Using an initial measured transmittance trc over a low-albedo surface ($\alpha = 0.1$), an effective optical depth τ is derived for each of two drop-size distributions. This intermediate quantity τ is then used to predict the transmittance of the observed cloud field over a different surface ($\alpha = 0.6$). The error in effective optical depth is typically 10%–15%, but the error in predicted transmittance ε_{trc} is usually less than 2%. The procedure of Fig. 7 was carried out for numerous cases of different zenith angles and surface albedos, and the results were similar to those shown in Fig. 7.

In all our computations, the model clouds consisted of liquid water droplets. However, we think our results are valid for ice clouds as well, by the following argument. The spectral absorption coefficient of ice (Warren 1984) is very similar to that of liquid water (Hale and Querry 1973) across the solar spectrum (they are plotted together for comparison by Dozier 1989, his Fig. 2b). Therefore the main reason that optical properties

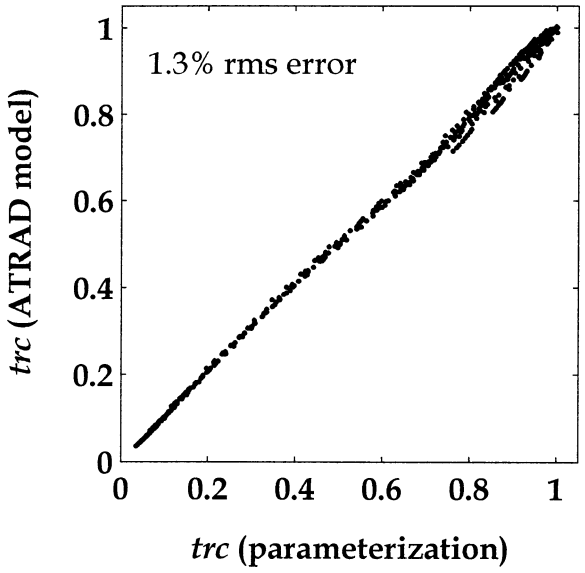

FIG. 5. Comparison of transmittance obtained from the radiative transfer model to that obtained from the parameterization, using a synthetic dataset, an rms error of 1.3% is shown.

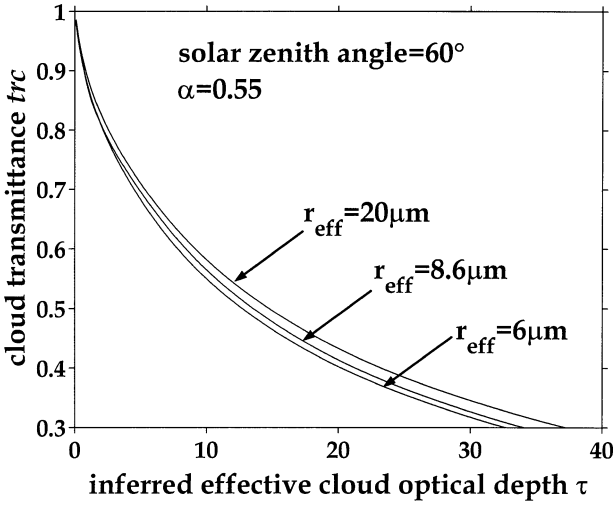

FIG. 6. Effect of assumed cloud droplet effective radius, r_{eff}, on the effective optical depth τ determined from the parameterization. To enable comparison with Fig. 7, τ (the dependent variable) is used as the abscissa. A larger effective radius of cloud droplets produces stronger forward scattering (larger asymmetry parameter) and hence a greater cloud transmittance than a cloud of the same optical depth with smaller effective radius.

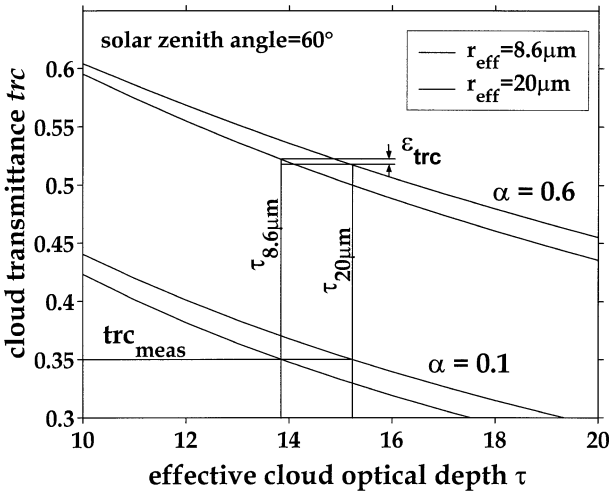

FIG. 7. Example of the error in derivation of cloud radiative properties due to lack of knowledge of the drop-size distribution. The cloud was observed over a surface of albedo 0.1, and the measured transmittance of solar radiation (trc) was 0.35. If we assume r_{eff} = 8.6 μm we obtain τ = 13.8. We estimate using the parameterization [Eq. (1)] that if this cloud were placed over a surface of albedo 0.6, it would have trc = 0.528. If we instead had larger drops (r_{eff} = 20 μm), we infer τ = 15.2, and estimate that if this cloud were placed over the high-albedo surface it would have trc = 0.512, very close to that estimated using the smaller drops. Lack of knowledge of r_{eff} in this case causes errors of 10%–15% in the intermediate quantity τ but only 2% in the prediction of solar transmittance in a different environment.

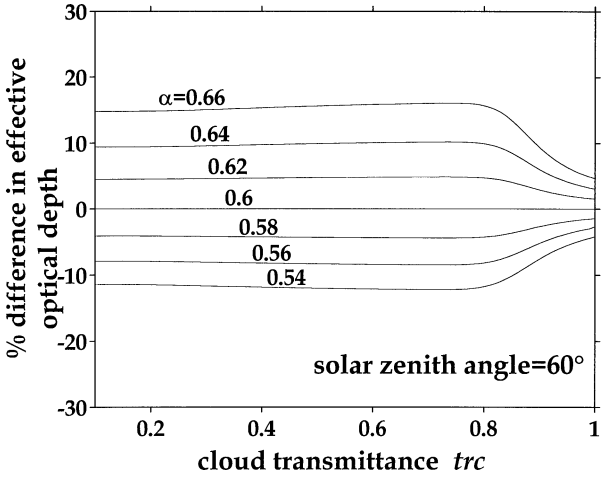

FIG. 8. Effect of errors in surface albedo estimates on the inference of effective cloud optical depth. This case is for a solar zenith angle of 60° and an erroneous assumed surface albedo of 0.6, with true surface albedos in the range 0.54–0.66.

of an ice cloud would differ from those of a water cloud of the same optical depth is that the ice particles are likely to be larger. Representing a nonspherical ice crystal by a collection of spheres having the same total volume and the same total surface area results in spheres with the same volume-to-area ratio (*V*/*A*) as the crystal. Using this representation, advocated by Grenfell and Warren (1999) and Fu (1996), any ice crystal shape can be described by a single effective radius for computation of absorption and scattering of radiation. This prescription results in little error for the shapes tested so far (hexagonal columns and plates; Neshyba et al. 2003). Using the equal-*V*/*A* description, the effective radii of crystals in ice clouds are typically 10–30 μm (Mahesh et al. 2001; Fu 1996; C. Schmidt and A. Heymsfield 2002, personal communication). Their effect is therefore represented by the example shown in Fig. 7.

Uncertainties in surface albedo also affect the values of cloud optical depth inferred using the parameterization. The albedo to be used in Eq. (1) is the actual albedo under the observed cloud, not what the albedo would be under clear sky. The effect on the parameterization of specifying an incorrect surface albedo is shown in Fig. 8 for a case where the estimated surface albedo was 0.6 but the true surface albedo was different by as much as 10%. An increase in surface albedo results in an increase in multiple reflections of incoming radiation. For a given measured cloud transmittance, if the estimated surface albedo entered into Eq. (1) is erroneously low, the inferred cloud optical depth will be too large. The errors introduced by uncertainties in surface albedo are greater for higher surface albedos. If the true albedo is 0.06 greater than the estimated albedo, the effective cloud optical depth is 15% too high, whereas if the true albedo is 0.06 lower than the estimated albedo, the effective cloud optical depth is only 11% too low. (The percent difference in derived τ is nearly independent of trc, but the absolute value of τ decreases as trc increases. For trc = 1.0, τ = 0, so the absolute difference vanishes.) Visual reports of ice-type distributions (as discussed later) are estimated to be accurate to $\pm$0.1 of ice concentration (A. Worby 2001, personal communication). We estimate that surface albedos derived from these reports are typically uncertain to $\pm$0.06 in albedo.

b. Spectral parameterization

The same form of the parameterization can also be used for narrow spectral intervals, with different coefficients for each interval. To do this we repeat the procedure described earlier, using spectral results from ATRAD, and derive coefficients for nine different wavelengths across the solar spectrum. These values are shown in Table 2. Using the parameterization instead of iterating through a radiative transfer model introduces an error of less than 1% at each of the specified wavelengths. Values are applicable at each specified wavelength, over the range of albedos, optical depths, and solar zenith angles used in the radiative transfer model. Attempts were made to fit the coefficients as functions of wavelength and hence generalize the parameterization across the whole solar spectrum. However, the spectral variation of downwelling irradiance, the spectral dependence of surface albedo of snow and ice, and the

TABLE 2. Coefficients in Eqs. (1), (2), and (3) found for nine different wavelengths λ, assuming $r_{\text{eff}} = 8.6$ μm. The last column gives the root-mean-square difference between values of cloud transmittance obtained from the spectral radiative transfer model and those obtained using the parameterization.

λ (nm)	a_1	b_1	b_2	b_3	k_1	k_2	k_3	c	d	Rms (%)
370	0.78	0.31	−0.0782	−0.9218	1.3	0.2000	0.8000	0.0835	0.0759	0.8
440	0.65	0.59	−0.1212	−0.8788	1.3	0.0229	1.1754	0.1008	0.0954	0.6
560	0.53	0.79	−0.1054	−0.8946	1.3	0.0409	1.2436	0.1153	0.1126	0.4
650	0.49	0.88	−0.1276	−0.8724	1.3	0.0436	1.1836	0.1215	0.1192	0.4
720	0.51	0.82	−0.1054	−0.8946	1.3	0.0575	1.3637	0.1307	0.1218	0.4
810	0.49	0.85	−0.0775	−0.9222	1.3	0.0531	1.0101	0.1324	0.1263	0.5
925	0.53	0.74	−0.0442	−0.9559	1.3	0.2000	0.8000	0.1426	0.1235	0.9
1050	0.48	0.99	−0.1975	−0.8025	1.3	0.1124	1.4246	0.1560	0.1482	0.7
1660	0.49	1.02	−0.0973	−0.9026	1.3	0.2209	1.7544	0.2318	0.1768	0.8

absorption characteristics of liquid water in clouds make such a generalization impractical. Downwelling irradiance varies by a factor of 100 over the region from 0.3 to 3.0 μm. Over the same spectral range the albedo of snow and ice surfaces decreases with wavelength and exhibits pronounced sharp minima in the infrared. Liquid water in clouds absorbs more strongly in the infrared. All these factors make it difficult to generalize the parameterization as a function of wavelength. We therefore offer parameterizations only for the nine discrete wavelengths in Table 2.

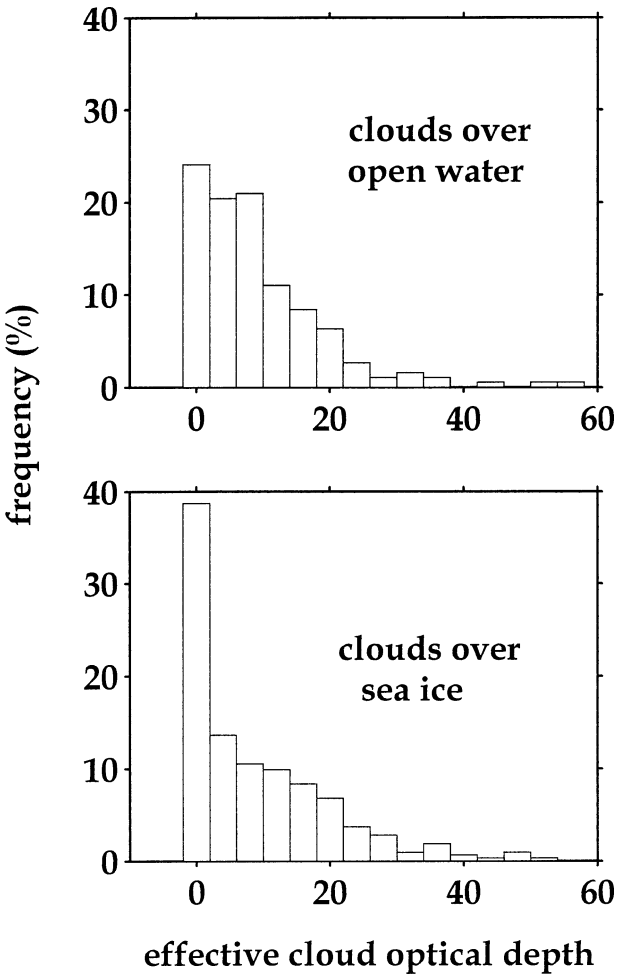

FIG. 9. Frequency distribution of cloud optical depth in the East Antarctic sea ice zone during a single ship voyage, derived using the broadband parameterization. An areal concentration of greater than two-tenths of sea ice is defined as sea ice; less than two-tenths is considered open water. The bin size is 4 units of optical depth. The bar at $\tau = 0$ represents clear sky.

5. Application to field data

The broadband parameterization is applied to measurements in the east Antarctic sea-ice zone during a 2-month springtime voyage in 1996. The data were collected on the research vessel *Aurora Australis* as part of the 49th Australian National Antarctic Research Expeditions (ANARE) between the latitudes of 44° and 69°S. Eppley pyranometers covering the spectral range from 0.3 to 2.8 μm measured downwelling irradiance at 10-s intervals for the duration of the voyage. Spectral irradiance was measured at infrequent intervals using a spectral radiometer covering the wavelength range 320–1060 nm. From these measurements raw cloud transmittances (trc) are obtained. An advantage of using measurements rather than model calculations to determine the clear-sky irradiance is that it does not require absolute calibration of the pyranometer. Furthermore, modeling errors are avoided.

Spectral surface albedos of different ice types in Antarctic sea ice have been measured in situ by Allison et al. (1993) and Brandt et al. (1999). Together with hourly visual observations, which include estimates of the fractional coverage of the ocean surface, the ice thickness, and the snow cover thickness for each of several ice types within 2 km of the ship (the relevant area for multiple reflections between the surface and low clouds), these albedos are used to determine the area-averaged surface albedo at a particular location. Using the broadband parameterization, effective cloud optical depth is derived. Figure 9 shows the frequency distribution of effective cloud optical depths obtained for this one voyage, using only those hourly observations performed while in the sea ice zone. The data are separated into two classes of surface type: ''open water,'' where the areal concentration of ice is at most 0.2, and ''sea

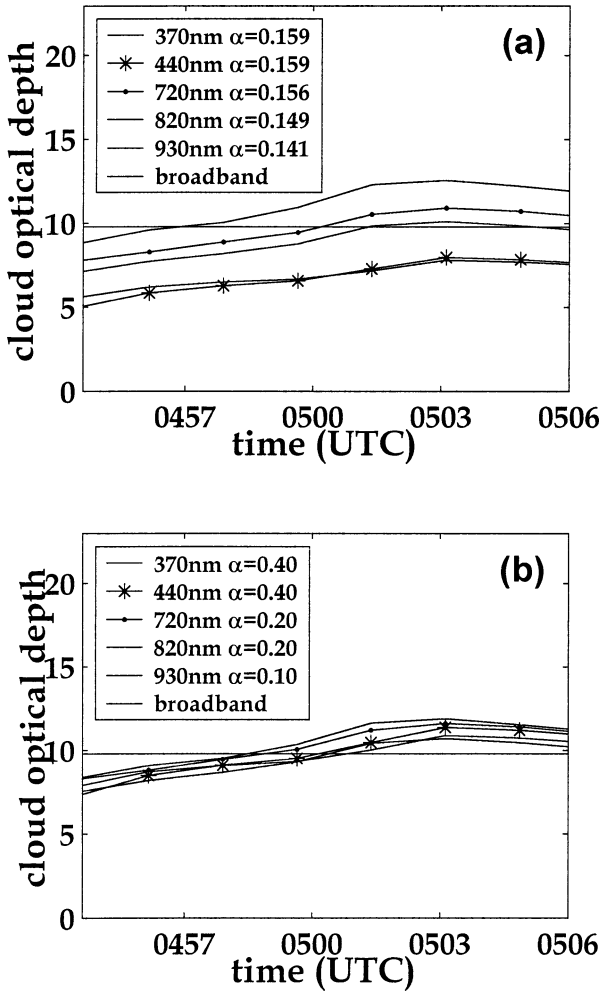

FIG. 10. Effective cloud optical depth (in the geometrics–optics limit) for a 15-min period with completely overcast sky, and a surface composed of one-tenth snow-covered first-year sea ice and nine-tenths open water. Values obtained using the broadband parameterization for a single observation at 0500 UTC are compared with those for five of the spectral parameterizations in (a) by assuming a weighted average of snow and water and in (b) by adjusting the spectral albedo (within ± 0.05) so that all spectral channels give the same optical depth (in the geometric-optics limit).

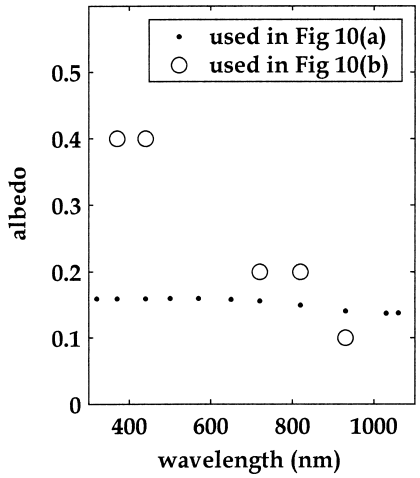

FIG. 11. Spectral surface albedos used to determine effective cloud optical depth in Fig. 10. The dotted line is based on the visual observation of ice types (one-tenth snow-covered ice, nine-tenths water), whereas the circles are the values of spectral albedo that cause the optical depth values to agree at each wavelength [Fig. 10(b)]. Some types of sea ice do have spectral albedos corresponding to the circles (Grenfell and Perovich 1984) but those types were not reported in the vicinity of the ship during the time of observation.

ice,'' where the areal concentration of ice is greater than 0.2. The figure shows that thin cloud is more prevalent in areas of open water and clear sky is more common over sea ice. The leftmost bin, $-2 < \tau < 2$, contains some derived optical depths that are negative (also shown later in Fig. 12). These are obtained from Eq. (1) when trc > 1. This may occur under a clear sky due to imperfect leveling of the pyranometers, and under a partly cloudy sky when the solar beam passes between clouds causing the downward solar irradiance to exceed the clear-sky irradiance.

We now investigate whether spectral and broadband measurements are consistent. To compare the spectral and broadband values of effective cloud optical depth a 15-min period was chosen when low concentrations of sea ice were present (and hence the area-averaged surface albedo was most accurate), and while the sky was completely overcast. The surface was nine-tenths water and one-tenth snow-covered ice. Figure 10 shows the effective cloud optical depth at five spectral wavelengths and compares them with the broadband value (measured at only one time, 0500 UTC). This comparison is done in two ways. In Fig. 10a, at each wavelength we use the visual observation of the fractional area covered by each ice type in the vicinity of the ship; at each of five wavelengths the albedo is computed as a weighted average of the measured spectral albedos of the different types (weighted by their area fractions). The albedos at these five wavelengths are used to compute five values of cloud optical depth. For the mixture of ice types reported present, the area-averaged albedo should be nearly constant with wavelength between 370 and 930 nm (dotted line in Fig. 11). The resulting computed optical depths (Fig. 10a), however, did not agree with each other. In Fig. 10b, we instead determine the spectral variation in surface albedo (also shown in Fig. 11) that would be necessary to calculate the same effective optical depth at all wavelengths.

The improvement in the comparison of effective optical depth in Fig. 10b results from using these latter spectral albedos that do correspond to some types of sea ice (Grenfell and Perovich 1984) but not to those ice types evident near the ship at this time. A possible, but speculative, explanation for the discrepancy is that the effective area of sea surface affecting the pyranometer measurement is greater for visible wavelengths than for near-infrared wavelengths. Because the cloud is more absorptive at longer wavelengths, photons at

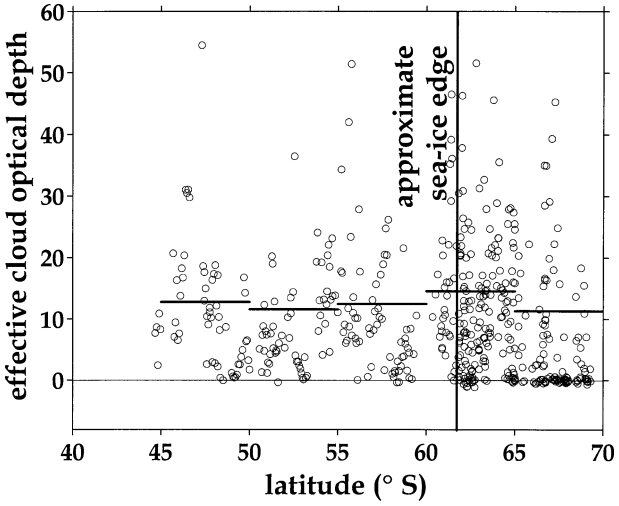

FIG. 12. Latitudinal variation of derived cloud optical depth during austral spring 1996 on a voyage from Australia to east Antarctica and return. Horizontal bars are averages of effective cloud optical depth over 5° of latitude, excluding cases of clear sky. The approximate edge of the sea ice was at 62°S. Points are plotted at hourly intervals, for daytime hours when the sun was at least 10° above the horizon. There are 514 points total.

these wavelengths cannot survive many bounces between cloud and surface. The near-IR downward irradiance may therefore be more dominated by the open water in the lead surrounding the ship, whereas for the visible wavelengths the relevant albedo is that of a larger area, extending beyond the lead into snow-covered floes. We have not attempted to model this effect. However, we emphasize that, for the typically mixed scenes in the sea ice zone, surface albedo is the least well-characterized of the variables required for use in both the broadband and spectral parameterization.

The latitudinal dependence of effective cloud optical depth for the duration of the voyage is shown in Fig. 12. One measurement per hour is plotted, for the entire voyage from 44°S to the edge of the Antarctic continent at 69°S. Observations at night or with the sun less than 10° above the horizon are excluded, leaving a total of 514 points. This figure shows the contrast between cloud optical depth over the open ocean and over the sea ice zone. The approximate edge of the sea ice was at 62°S. It is evident that there are far more instances of clear sky over the sea ice than over the ocean, probably due in part to the decrease in ocean–atmosphere moisture exchange in the sea ice zone. However the mean values of cloud optical depth show little latitudinal variation.

6. Conclusions

A simple but accurate parameterization has been developed relating raw cloud transmittance trc to cloud optical depth τ, surface albedo α, and solar zenith angle θ. The parameterization was derived using the measured spectral albedos of snow, ice, and water; the same form of parameterization could be used for various land surfaces, but with different coefficients derived for their spectral shapes.

The parameterization is intended for use in the analysis of measured surface irradiance to obtain an effective cloud optical depth τ from measurements of trc. The inferred value of τ is an inherent property of the cloud field, allowing computation of cloud transmittance for other conditions of solar illumination and surface albedo, thus allowing instantaneous point measurements to be used for computation of diurnal-average and seasonal-average cloud radiative forcing. The parameterization may also find use in climate modeling.

Acknowledgments. We thank Istvan Laszlo (University of Maryland) for helping us implement the ATRAD model. We thank Ian Allison of the Australian Antarctic Division for sponsoring the fieldwork for this project, and Tom Grenfell, Tony Worby, Thomas Ackerman, Charles Long, and Warren Wiscombe for discussions. This work was supported by NSF grants OPP-95-27244 and OPP-98-15156, and by a NASA Earth System Science Fellowship to Melanie Fitzpatrick.

REFERENCES

Allison, I., R. E. Brandt, and S. G. Warren, 1993: East Antarctic sea ice: Albedo, thickness distribution, and snow cover. *J. Geophys. Res.,* **98,** 12 417–12 429.

Ayers, G. P., and J. L. Gras, 1991: Seasonal relationship between cloud condensation nuclei and aerosol methanesulphonate in marine air. *Nature,* **353,** 834–835.

Barker, H. W., T. J. Curtis, E. Leontieva, and K. Stamnes, 1998: Optical depth of overcast cloud across Canada: Estimates based on surface pyranometer and satellite measurements. *J. Climate,* **11,** 2980–2994.

Boers, R., and P. B. Krummel, 1998: Microphysical properties of boundary layer clouds over the Southern Ocean during ACE 1. *J. Geophys. Res.,* **103,** 16 651–16 633.

——, A. van Lammeren, and A. Feijt, 2000: Accuracy of cloud optical depth retrievals from ground-based pyranometers. *J. Atmos. Oceanic Technol.,* **17,** 916–927.

Brandt, R. E., C. S. Roesler, and S. G. Warren, 1999: Spectral albedo, absorptance, and transmittance of Antarctic sea ice. Preprints, *Fifth Conference on Polar Meteorology and Oceanography,* Dallas, TX, Amer. Meteor. Soc., 456–459.

Briegleb, B., and V. Ramanathan, 1982: Spectral and diurnal variations in clear sky planetary albedo. *J. Appl. Meteor.,* **21,** 1160–1171.

Cess, R. D., and Coauthors, 1990: Intercomparison and interpretation of climate feedback processes in 19 atmospheric general circulation models. *J. Geophys. Res.,* **95,** 16 601–16 615.

Dozier, J., 1989: Spectral signature of alpine snow cover from the Landsat Thematic Mapper. *Remote Sens. Environ.,* **28,** 9–22.

Fu, Q., 1996: An accurate parameterization of the solar radiative properties of cirrus clouds for climate models. *J. Climate,* **9,** 2058–2082.

Gardiner, B. G., 1987: Solar radiation transmitted to the ground through cloud in relation to surface albedo. *J. Geophys. Res.,* **92,** 4010–4018.

Grenfell, T. C., and D. K. Perovich, 1984: Spectral albedos of sea ice and incident solar irradiance in the southern Beaufort Sea. *J. Geophys. Res.,* **89,** 3573–3580.

——, and S. G. Warren, 1999: Representation of a nonspherical ice

particle by a collection of independent spheres for scattering and absorption of radiation. *J. Geophys. Res.*, **104,** 31 697–31 709.
——, ——, and P. C. Mullen, 1994: Reflection of solar radiation by the Antarctic snow surface at ultraviolet, visible and near-infrared wavelengths. *J. Geophys. Res.*, **99,** 18 669–18 684.
Hahn, C. J., W. B. Rossow, and S. G. Warren, 2001: ISCCP cloud properties associated with standard cloud types identified in individual surface observations. *J. Climate*, **14,** 11–28.
Hale, G. M., and M. R. Querry, 1973: Optical constants of water in the 200-nm to 200-μm wavelength region. *Appl. Opt.*, **12,** 555–563.
Jayaweera, K. O. L. F., and T. Ohtake, 1973: Concentration of ice crystals in Arctic stratus clouds. *J. Rech. Atmos.*, **7,** 199–207.
Labs, D., and H. Neckel, 1970: Transformation of the absolute solar radiation data into the International Practical Temperature Scale of 1968. *Solar Phys.*, **15,** 79–87.
Leontyeva, E., and K. Stamnes, 1994: Estimations of cloud optical thickness from ground-based measurements of incoming solar radiation in the Arctic. *J. Climate*, **7,** 566–578.
——, and ——, 1996: Remote sensing of cloud optical properties from ground-based measurements of transmittance: A feasibility study. *J. Appl. Meteor.*, **35,** 2011–2022.
Lubin, D., and A. S. Simpson, 1997: Measurement of surface radiation fluxes and cloud optical properties during the 1994 Arctic Ocean section. *J. Geophys. Res.*, **102,** 4275–4286.
Mahesh, A., V. P. Walden, and S. G. Warren, 2001: Ground-based infrared remote sensing of cloud properties over the Antarctic Plateau. Part II: Cloud optical depths and particle sizes. *J. Appl. Meteor.*, **40,** 1279–1294.
McClatchey, R. A., R. W. Fenn, J. F. A. Selby, F. E. Volz, and J. S. Garing, 1972: Optical properties of the atmosphere. 3d ed. Air Force Geophysics Laboratory Rep. AFCRL-72-0497, Hanscom, MA, 108 pp.
Neckel, H., and D. Labs, 1984: The solar radiation between 3300 and 12,500 Angstorms. *Solar Phys.*, **90,** 205–258.
Neshyba, S. P., T. C. Grenfell, and S. G. Warren, 2003: Representation of a nonspherical ice particle by a collection of independent spheres for scattering and absorption of radiation: II. Hexagonal columns and plates. *J. Geophys. Res.*, **108,** 4448, doi:10.1029/2002JD003302.
Nussenzveig, H. M., and W. J. Wiscombe, 1980: Efficiency factors in Mie scattering. *Phys. Rev. Lett.*, **45,** 1490–1494.
Press, W. H., S. A. Teukolsky, W. T. Vetterling, and B. P. Flannery, 1992: *Numerical Recipes: The Art of Scientific Computing*. Cambridge University Press, 994 pp.
Reist, P. C., 1993: *Aerosol Science and Technology*. McGraw-Hill, 379 pp.
Rossow, W. B., and R. A. Schiffer, 1999: Advances in understanding clouds from ISCCP. *Bull. Amer. Meteor. Soc.*, **80,** 2261–2287.
Schuster, A., 1905: Radiation through a foggy atmosphere. *Astrophys. J.*, **21,** 1–22.
Shine, K. P., 1984: Parameterisation of the shortwave flux over high albedo surfaces as a function of cloud thickness and surface albedo. *Quart. J. Roy. Meteor. Soc.*, **110,** 747–764.
Stokes, G. M., and S. E. Schwartz, 1994: The Atmospheric Radiation Measurement (ARM) Program—Programmatic background and design of the cloud and radiation test-bed. *Bull. Amer. Meteor. Soc.*, **75,** 1201–1221.
Warren, S. G., 1982: Optical properties of snow. *Rev. Geophys. Space Phys.*, **20,** 67–89.
——, 1984: Optical constants of ice from the ultraviolet to the microwave. *Appl. Opt.*, **23,** 1206–1225.
——, C. J. Hahn, J. London, R. M. Chervin, and R. L. Jenne, 1986: Global distribution of total cloud cover and cloud type amounts over land. NCAR Tech. Note TN-273+STR, Boulder, CO, 29 pp. and 200 maps.
——, ——, ——, ——, and ——, 1988: Global distribution of total cloud cover and cloud type amounts over the ocean. NCAR Tech. Note TN-317+STR, Boulder, CO, 42 pp. and 170 maps.
Wiscombe, W. J., 1975: Solar radiation calculations for Arctic summer stratus conditions. *Climate of the Arctic*. G. Weller and S. A. Bowling, Eds., University of Alaska Press, 245–254.
——, 1980: Improved Mie scattering algorithms. *Appl. Opt.*, **19,** 1505–1509.
——, R. M. Welch, and W. D. Hall, 1984: The effects of very large drops on cloud absorption. Part I: Parcel models. *J. Atmos. Sci.*, **41,** 1336–1355.